Fibers and Polymers 2021, Vol.22, No.9, 2464-2474
DOI 10.1007/s12221-021-1210-8

ISSN 1229-9197 (print version)
ISSN 1875-0052 (electronic version)

Novel Synthesis of Ag NPs on Polymer Fabrics by a Green Method for Antibacterial Performance

Zhi Jin[1], Chaofan Shi[1], Minwei Li[3], Jinru Ji[3], Shoufeng Wang[2]*, and Xiwen Zhang[1]*

[1]*State Key Laboratory of Silicon Materials, School of Materials Science and Engineering, Zhejiang University, Hangzhou 310027, China*
[2]*Institute of Pharmaceutical Biotechnology, School of Medicine, Zhejiang University, Hangzhou 310058, China*
[3]*State Key Laboratory for Diagnosis and Treatment of Infectious Diseases, National Clinical Research Center for Infectious Diseases, Collaborative Innovation Center for Diagnosis and Treatment of Infectious Diseases, The First Affiliated Hospital, College of Medicine, Zhejiang University, Hangzhou 310013, China*
(Received October 13, 2020; Revised December 29, 2020; Accepted January 5, 2021)

Abstract: In the present work, silver nanoparticles (Ag NPs) were deposited on PET fabrics by a green method. The fabric samples were firstly treated by ambient air cold plasma. Then, the Ag_2O nanoparticles were deposited on the surface of the samples assisted by ultrasonic spraying technology. Finally, the Ag_2O nanoparticles were *in-situ* reduced into Ag NPs by H_2 DBD cold plasma. Results of SEM, EDS, high-resolution XPS and TEM analyses confirmed that Ag_2O were completely reduced into Ag NPs. Thermogravimetry analysis (TGA) and tensile test were used to evaluate the thermodynamic properties and mechanical properties of the Ag NPs deposited PET fabrics. The antibacterial experiments indicted that the as-prepared Ag NPs-deposited fabrics exhibited considerable antibacterial activity against both *S. aureus* and *E. coli*. Therefore, these materials have promising applications in the medicinal filed as well as in human daily life to relieve the many problems caused by bacteria.

Keywords: Ag nanoparticles, PET fabrics, DBD cold plasma, Antibacterial activity, Green synthesis

Introduction

The emergence of novel pathogenic microorganisms as well as their increasing resistance to antibiotics have become major global issues facing humanity [1,2]. Infectious diseases caused by multi-resistant bacteria given the urgent need to develop new antimicrobial agents [3-5].

Silver nanoparticles (Ag NPs) are one of the attractive agents against multiple pathogenic microorganisms [6]. The bacterial resistance to silver-based antibacterial agents has developed slowly relative to the resistance to traditional antibiotics, because of the complex and multiple mechanism of the inhibitory effect of silver [7]. One of the widely accepted explanations is that silver ions can accumulate on the negatively charged membrane of bacteria, thereby damaging the biological function of cell membranes, and they may even react with the thiol groups of proteins, giving rise to bacterial inactivation [8-10]. However, silver ions-based antibacterial agents are extremely sensitive to electrolytes, and rapidly become ineffective via reactions with anions [8,11]. On the other hand, the burgeoning nanotechnology makes Ag NPs a promising candidate for new, effective antibacterial agents [12-14]. They could potentially act as a sustained source of ions, continuously releasing them by partial surface oxidation, while simultaneously directly damaging bacterial membranes [15,16].

The aggregation of free Ag NPs could result in an obvious decrease in their toxicity to bacteria. Dispersing agents such as citrate and polyvinyl pyrrolidone (PVP) are accordingly often employed to improve the stability of Ag NPs in solution [10,17-19]. Recently, various matrix materials, such as paper, textiles, and ceramics decorated with Ag NPs have attracted much attention [20-24]. These immobile forms of Ag NPs have favorable dispersibility and are easily recycled, compared with the free Ag NPs. Ag NPs modified bandages have already been used in surgical treatment for wound repair [25-27]. Polymer fibers like polypropylene (PP) and polyethylene terephthalate (PET) with high strength-to-weight ratio and low cost in products with high resistance towards corrosion, are used for a wide variety of applications in many fields like domestic and medical protective products [28]. However, chemical reductants or adhesion agents are indispensable when depositing Ag NPs on the hydrophobic fibers [29,30]. Some chemical agents are toxic, expensive, and are especially harmful to the environment.

Atmospheric cold plasma technology has proven to be useful among other things, for decreasing the water contact angle of polymers without changing their bulk properties [31-33]. Researchers attribute this reduction of water contact angle to the formation of the hydrophilic groups such as -OH, C=O, COO-, -OOH, -COOH, $-NH_2$, and -NH at the surface of the polymers [34,35].

Dielectric barrier discharge (DBD) under hydrogen is a new and green method for *in-situ* preparing metal nanoparticle decorated fabrics. Ag NPs could be prepared on fabrics by DBD cold plasma process efficiently, regardless of their surface properties.

*Corresponding author: sfwang@zju.edu.cn
*Corresponding author: zhangxw@zju.edu.cn

Recently, plasma plays an increasingly important role in fabric modification with Ag NPs. However, in many reports, plasma is only used to activate the surface of fabrics. Low pressure oxygen plasma can activate the cotton fabric, and help to form silanols on the surface. Ag NPs was produced by thermal reduction of excess Ag^+ from an aqueous solution of silver N-(2-ethylhexyl) carbamate on the fibrous cotton surface at 130 °C [36]. In another study, plasma deposition is also used in preparing Ag NPs decorated PET fabrics. A layer of organosilicon thin film was deposited on the surface of PET to adsorb Ag NPs the by plasma treatment. Then the sample was immersed in the Ag NPs suspension. Finally, another layer of organosilicon thin film was deposited on surface of the fabric by plasma treatment to improve the durability [37]. It was also reported that Ag NPs were deposited on *meta*-aramid fiber paper (MAFP) by combining oxygen plasma treatment and electroless silver plating. The oxygen plasma was used to activate the surface and lead the high interface binding between MAFP and Ag NPs. The Ag NPs were prepared by reducing ammoniacal silver nitrate solution [38]. Plasma was utilized to activate the surface of fabrics in many experiments. However, methods to prepare Ag NPs in these studies are complex, which usually need reducing agents, binding agents or stabilizing agents. This problem can be easily solved by preparing Ag_2O nanoparticles on the surface of fibers and then *in-situ* reducing them by H_2 DBD plasma.

Herein, a green, efficient method for *in-situ* preparation of highly dispersed Ag NPs modified fabrics involving cold plasma surface modification, ultrasonic spraying-assisted particle deposition and H_2 DBD plasma reduction is studied. Compared with other studies, Ag NPs can be *in-situ* prepared on the surface of fabric without using any chemical additives. The antibacterial effects of the modified fabrics are also evaluated.

Experimental

Materials

In the present experiment, commercially available polymer fabric (PET, non-woven fabric, average fiber diameter 10 μm, 160 g/m^2) was used. The fabric was dipped into ethanol solution and cleaned with ultrasonic washer for 30 minutes and then washed repeatedly with distilled water to remove the impurities and dried in air before use. Silver nitrate (AR) and ammonium hydroxide (AR) were obtained from Sinopharm Chemical Reagent Co., Ltd.. All the chemical reagents were used without further purification.

Atmospheric Cold Plasma Treatment

The hydrophobic fabric was first subjected to surface modification treatment by ambient air cold plasma to increase the surface energy. A homemade cold plasma system, shown in Figure 1(a), was used for this pretreatment process. The environmental humidity was controlled in the range of 40 % to 50 %, and the temperature was about 25 °C during the experiment. An electro-mechanical system was employed to affix the fabric and enable it to slide back and forth in the horizontal ceramic plane at a controlled speed of 1 cm/s. A high alternating pulse voltage were applied between the ceramic electrode and the ceramic plate by an electrical power transformer with an input power of 37.5 W. The air breakdown and discharge were induced by the high voltage alternating current power source in the narrow gap between the two dielectric layers, which created a homogeneous high-energy density plasma layer. The fabric samples passed through this plasma layer, with a reciprocating motion. After 3 minutes of ambient air cold plasma treatment, the sample was immersed into the $AgNO_3$ solution for 10 minutes with magnetic stirring. Then, the sample was affixed to plastic grill in a light-blocking container.

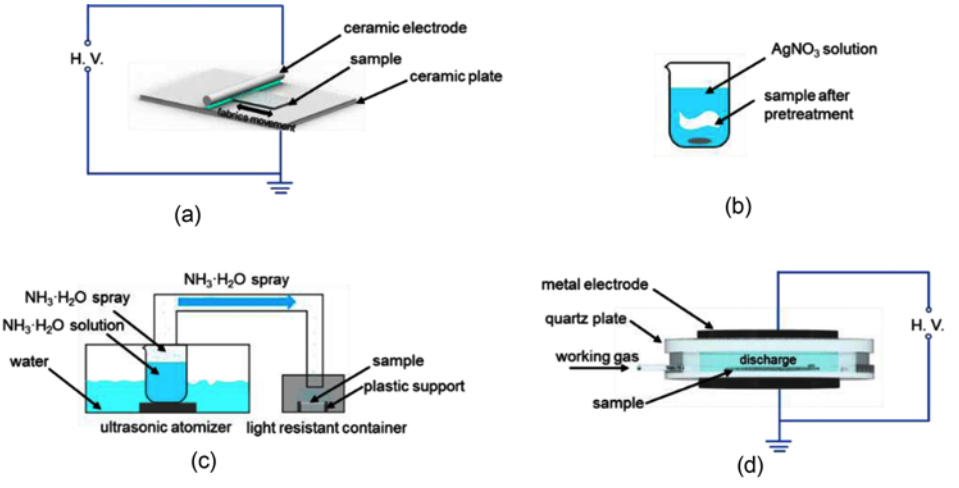

Figure 1. Schematic for the synthesis of Ag NPs-modified fabrics; (a) ambient air cold plasma treatment, (b) immersed in $AgNO_3$ solution, (c) ultrasonic atomization, and (d) dielectric barrier discharge cold plasma treatment.

Precipitation Reaction Assisted by Ultrasonic Atomization

The ultrasonic atomization technology was utilized in precipitation reaction. Briefly, NH_3 H_2O spray was created by an ultrasonic atomizer (YUWELL 402B) and transported continuously to the light-blocking container, as shown in Figure 1(c). This process lasted for 5 minutes. The resulting samples were subsequently rinsed with deionized water for several times to remove the unreacted chemical reagents, and then dried at 80 °C for 30 minutes. The concentration of $NH_3 \cdot H_2O$ solution used in the experiment was 0.5 M.

Reduction of Ag NPs by H_2/Ar DBD Plasma

The homemade DBD cold plasma system was shown in Figure 1(d). Two plane-parallel metal electrodes covered by a quartz plate as the dielectric layer, respectively. The electrodes gap width was controlled in 3 mm to ensure uniform discharge and stable plasma operation. When the working gas flowed into the narrow chamber, the high potential difference applied on the two metal plates would give rise to gas breakdown and ignite the discharge. Thus, metal oxides can be reduced into their elemental states by of the H radicals or atoms produced in the plasma. In the experiment, the mixture of H_2 and Ar (gas volume fraction of 5 % and 95 %, respectively) was introduced into the reactor at a flow rate of 50 m*l*/min for 2 minutes to purge the reactor. The duration of the plasma treatment was limited to 10 s with the flow rate of the working gas controlled at 30 m*l*/min. The input power of the electrical power transformer was 22.5 W. The concentrations of $AgNO_3$ solution in the present experiment were variously 0, 11.8 mM, 23.6 mM, 35.3 mM, 47.2 mM, and 59.0 mM, and the corresponding samples obtained were denoted as Ag0, Ag1, Ag2, Ag3, Ag4 and Ag5, respectively.

Characterization

X-ray photoelectron spectroscopy (XPS) was used to investigate the chemical changes arising out of the plasma treatment, using a VG ESCALAB MARK II spectrometer with an Mg Kα (1253.6 eV) X-ray source, and collected spectral data were calibrated by the C 1s peak at 284.6 eV. The hydrophilicity of these polymer film surfaces was studied by contact angle measurements using a video-based, contact angle measuring device (OCA 20, Dataphysics, Germany). Deionized water was used as the probe liquid in all measurements. Field emission scanning electron microscopy (FESEM, Hitachi SU-70) was used to characterize the microstructures of the cotton fibers and Ag NPs particles. Energy dispersive spectroscopy (EDS) was performed on the SEM. UV-Vis diffuse reflectance spectra of samples were obtained using a UV-Vis spectrophotometer (Shimadzu UV-3150 UV-Vis-NIR spectrophotometer, Japan). $BaSO_4$ was used as a reflectance standard in the UV-Vis diffuse reflectance experiments. The sample morphology was observed by transmission electron microscopy (FEI Talos-S) and high-resolution transmission electron microscopy (HRTEM) at a 200 kV accelerating voltage. The concentration of Ag NPs and Ag ions were determined by an inductively coupled plasma source mass spectrometer (ICP, Agilent 7700X). The Colorimeter (SC-10, ThreeNH, China) was used to measure the colorimetric data CIELAB color space values (L*, a*, b*) of the treated fabrics. And the test light source type is D65. Thermogravimetric analysis (TGA, SDT-Q600) was carried out to characterize the decomposition and thermal stability of samples. 10 mg of sample Ag0 and Ag3 were placed in an alumina crucible and heated from 20 °C to 800 °C under nitrogen atmosphere, with the heating rate of 20 °C/min. To determine the tensile strength and elongation of the sample. the fabric tensile tests were conducted by electronic universal testing machine (CMT6103, MTS, America). There is no orientation requirement for non-woven fabric when preparing the tensile sample. The tensile samples with a size of 50 mm × 250 mm and a gauge length of 50 mm. The tensile rate is 100 mm/min. Each test is repeated three times.

Bacterial Strains

The antibacterial activity of fabrics with Ag nanocomposites was tested against two bacterial strains viz. *Escherichia coli* (ATCC 11229) and *Staphylococcus aureus* (ATCC 6538). *E. coli* belongs to gram-negative bacteria, while *S. aureus* belongs to gram-positive bacteria. The strains were purchased from China Center of Industrial Culture Collection (CICC) and preserved in liquid nitrogen.

Antibacterial Experiment

The standard shaking-flask method (ASTM-E2149-01) against *E. coli* and *S. aureus* was performed to evaluate the antimicrobial activities of the samples in this experiment. Different mass of sample Ag0, Ag1, Ag2, Ag3, Ag4 and Ag5 were added into Erlenmeyer flasks with 50 m*l* bacteria solution with an initial bacterial liquid concentration of about 1×10^7 CFU/m*l*. The flasks were then put into Wrist Action flasks. The bacteria were shaking in the Wrist Action flasks at 37 °C at the maximum speed for 1 h. After shaking-flask culture, the final concentrations of bacteria were calculated by dilution methods.

In addition, the minimum inhibitory concentration (MIC) value of the sample Ag3 was determined to evaluate the antibacterial activity. Different concentrations of the sample Ag3 (the front and back of the samples were sterilized by ultraviolet light for 20 minutes) were mixed with 2 m*l* bacterial solution in sterilized test tubes with a bacterial liquid concentration of about 5×10^5 CFU/m*l*. After mixing, these test tubes were placed in an incubator at 37 °C for 20 h. A test tube having only growth media and bacteria served as the control. The experiment was carried out under aseptic conditions. For this test, 10 mg to 60 mg weights of the sample Ag3 were immersed in 2 m*l* of bacterial solution. The minimum concentration of the compound which

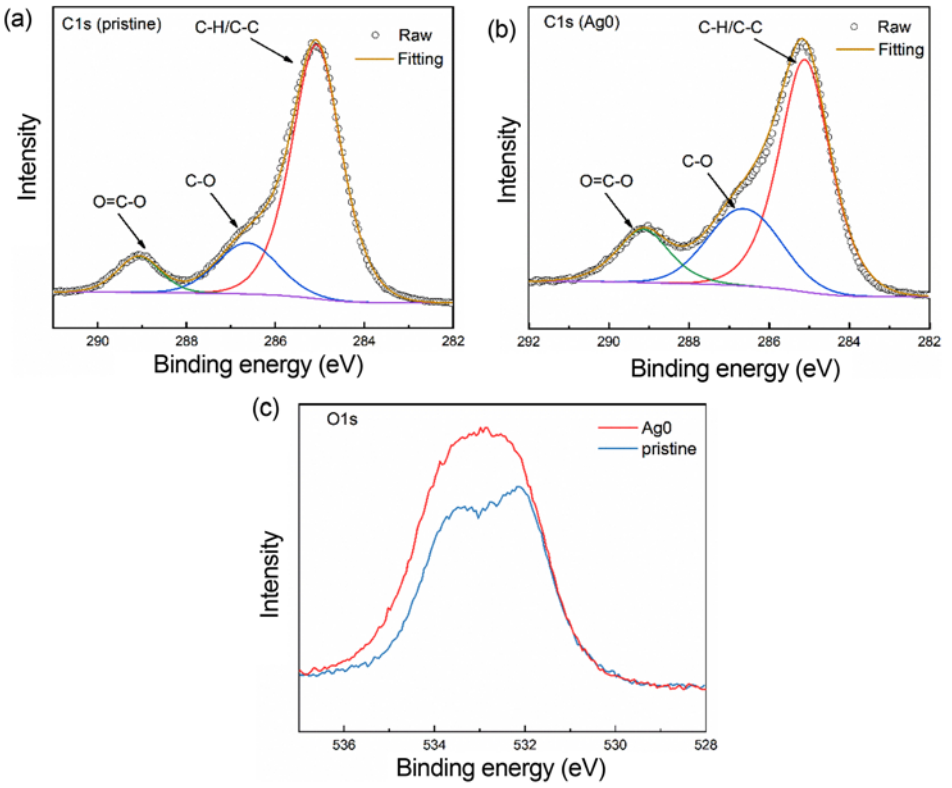

Figure 2. High-resolution XPS spectra of C1s; (a) pristine fabric, (b) Ag0, and O1s (c).

inhibited the growth of the respective organisms was considered as the MIC. The assay was carried out in triplicate to reduce the measurement error. The MIC was defined as the lowest concentration of sample at which no microbial growth was detected by visual inspection.

Results and Discussion

High-resolution XPS analyses of C1s and O1s confirmed the composition and the modification of the surface, shown in Figure 2. The pristine fabric and sample Ag0 show the same peak positions at 285.0 eV, 286.7 eV and 289.0 eV which are attributed to C-C/C-H, C-O and O-C=O, respectively [39]. As shown in Figure 2(c), the oxygen content in the sample Ag0 is higher than pristine fabric. This is due to the introduction of abundant oxygen-containing active groups during the ambient air cold plasma treatment process [40,41]. The ratio of the peak area of O1s and C1s (the O/C atomic ratio) is used to characterize the changes in the surface state of the samples. The O/C atomic ratio of the pristine fabric is 20.77 % / 79.23 % = 0.262. The O/C atomic ratio of the sample Ag0 is 26.95 % / 73.05 % = 0.369, which is significantly increased compared to the pristine fabric, indicating that the oxygen-containing polar groups on the surface of the fabric increased after ambient air cold plasma treatment.

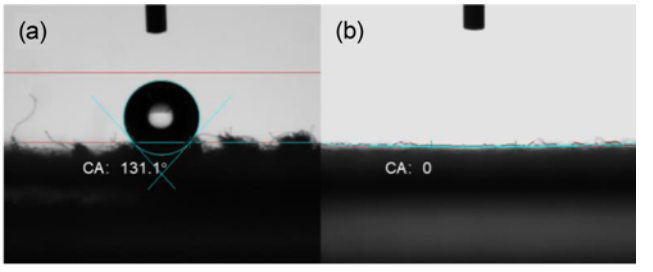

Figure 3. Water contact angle of (a) the pristine blended fabric and (b) Ag0.

The water contact angle (C.A.) test was employed to evaluate the wettability of the fabrics. Most of common PET fabrics are of poor wettability, low surface energy and lack of polar groups. As shown in Figure 3, the water C.A. of pristine fabrics is 131.1 °. It is quite difficult to functionalize PET fibers by simple liquid phase reaction. In addition, the molecular chain structure of PET is not favorable to the Ag_2O particles attaching on the fibers without a modification step.

Figure 3(b) shows the water C.A. of the fabrics after a 5-minute ambient air cold plasma treatment. The water drop was immediately absorbed by the fabric entirely (Supplementary information). Since the oxygen-containing groups introduced by plasma treatment are all hydrophilic

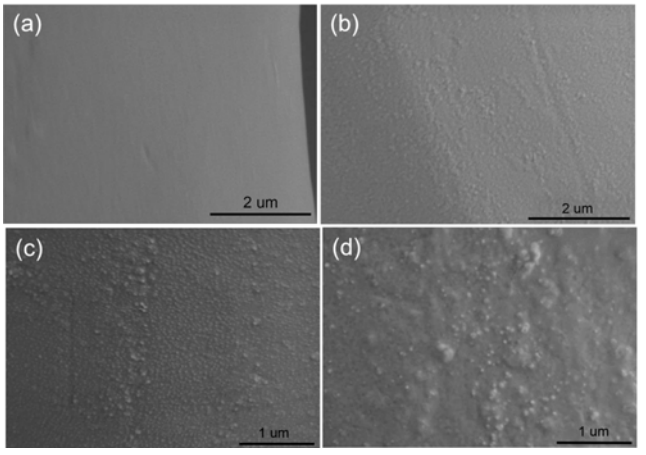

Figure 4. FESEM images of (a) pristine fabric, (b) Ag1, (c) Ag2, and (d) Ag3.

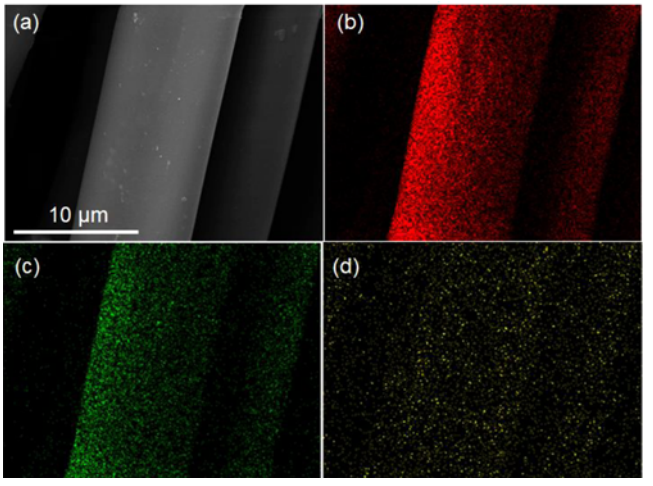

Figure 5. (a) SEM images of sample Ag3, and element mapping images of (b) C, (c) O, and (d) Ag.

oxygen-containing end-groups [42]. Thus, the hydrophilic properties of the fabric are significantly improved. The decrease in water C.A. indicates the formation of hydrophilic groups on the surface of sample Ag0, which is consistent with the increase of O/C atomic ratio. The plasma reacts with the topmost layers of the fabrics, which promotes chain scission and improves the wettability of the fabrics. Polar groups are interlocked by the free radicals on the surface of the fabrics [42].

The morphologies of pristine fabric, the samples Ag1, Ag2, and Ag3 are shown in Figure 4. It is obvious that after ambient air cold plasma treatment, the fabrics exhibit a more irregular surface with drop-like or nodule structures, which corresponds to the results of an earlier study [43]. The rough surface could provide nucleation sites for the precipitation reaction. Nanoscale particles without aggregation could also be observed from the samples Ag1, Ag2 and Ag3.

In Figure 5, the SEM images and corresponding EDS mapping diagrams of sample Ag3 revealed that the elemental Ag was well and uniformly distributed on the surface of the fabric fibers without aggregation. The amount of Ag in the samples measured by ICP is listed in Table 1. As the results show, the content of silver in samples gradually increased along with the increase of Ag NPs.

After ambient air cold plasma treatment, the subsequent processing can be described by the following reactions:

$$2AgNO_3 + 2NH_3\,H_2O \rightarrow Ag_2O + 2NH_4NO_3 + 2H_2O \quad (1)$$

$$e^* + Ar \rightarrow Ar^* + e \quad (2)$$

$$e^* + H_2 \rightarrow H_2^* + e \quad (3)$$

$$2Ag^+ + H_2^* + 2e \rightarrow 2Ag + H_2 \quad (4)$$

Where e* is the electron with high energy, and H_2* and Ar*, the excited state of H_2 and Ar, respectively. This

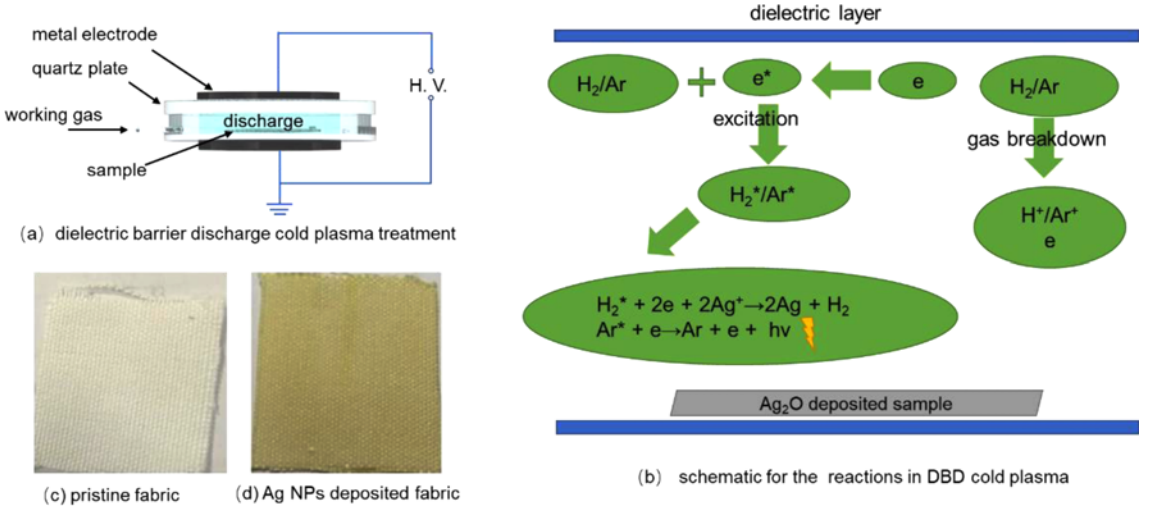

Figure 6. (a), (b) Schematic for the reactions during DBD cold plasma treatment, (c) the pristine fabric, and (d) as-prepared Ag NPs deposited fabric.

process is shown schematically in Figure 6.

When the NH_3 H_2O spray flows into the light-blocking container, the reaction (1) would immediately take place on the surface of the fibers. The irregular surface of the fibers could apply sites for nucleation and improve the adhesion of Ag_2O nanoclusters.

Reactions (2), (3) and (4) demonstrate the main process during the H_2/Ar DBD cold plasma treatment. The high potential difference applied on the metallic electrodes creates an electric field in the narrow gap between the quartz glass plates. Electrons gain energy, accelerate along the electric field, and collide with heavy particles (e.g. atoms, nucleus, or molecule) which would cause an energy exchange between the electrons and the heavy particles [44, 45]. As a result, gas breakdown and excitation in the plasma system generate abundant excited H radicals or atoms with high reducibility. Ag_2O nanoparticles could then *in-situ* transform into Ag NPs on the fabric in the H_2/Ar plasma.

High resolution XPS for Ag3d and Ag Auger, as well as UV-Vis diffuse reflectance spectra were utilized to verify the existence of metallic Ag after H_2 DBD cold plasma. In order to prove the effects of the ambient air cold plasma treatment, the sample Fab-Ag was prepared by the same way as the sample Ag3, but without the pretreatment.

As shown in Figure 7, the spectra of high resolution XPS of Ag3d exhibit two peaks, i.e. Ag 3d3/2, and Ag 3d5/2, located at 374.3 eV and 368.3 eV respectively. Their spin energy separation is 6 eV, which indicates that Ag exists in its metallic state [45]. The spectrum of sample Fab-Ag also shows the two peaks at the same locations with very low intensity compared with those of the spectra of the samples Ag1, Ag2, and Ag3, which indicates that the ambient air cold plasma treatment helps the Ag NPs to adhere to the polymer fibers.

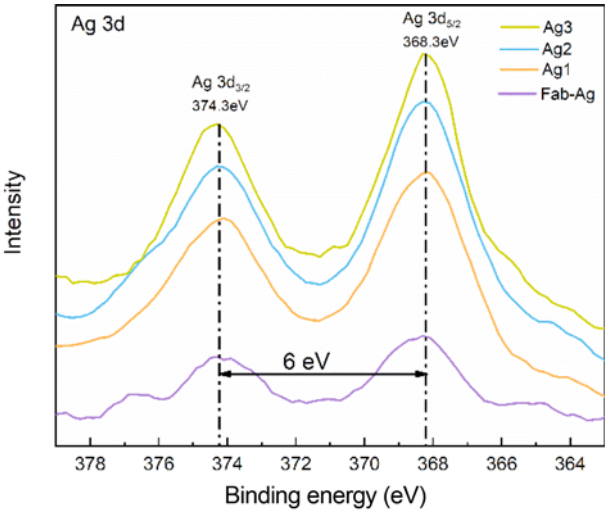

Figure 7. High-resolution XPS spectra of Ag3d of the samples Fab-Ag, Ag1, Ag2, and Ag3.

The deconvolution of the Auger spectra (MNN) of sample Ag1, Ag3, and Ag5 was shown in Figure 8. All the samples exhibit two peaks at 351.8 eV and 357.8 eV, corresponding with the Auger kinetic energy of metallic Ag (M5N45N45 and M4N45N45) [46]. The kinetic energy peaks of Ag_2O locating at 356.6 eV and 350.6 eV [47], do not appear in Figure 8. Thus, Ag only exists as the elementary substance.

The UV-Vis DRS spectra of samples Fab-Ag, Ag0, Ag1, Ag2, and Ag3 are shown in Figure 9. Studies have revealed that Ag NPs absorb electromagnetic radiation in the visible region (380-450 nm) via a phenomenon known as the excitation of the localized surface plasmon resonance (LSPR) [48-50]. The LSPR peaks around 415 nm can be observed from the samples Ag1, Ag2, and Ag3. The intensities of the SPR peaks increase with the corresponding increasing molar concentration of the $AgNO_3$ solution used,

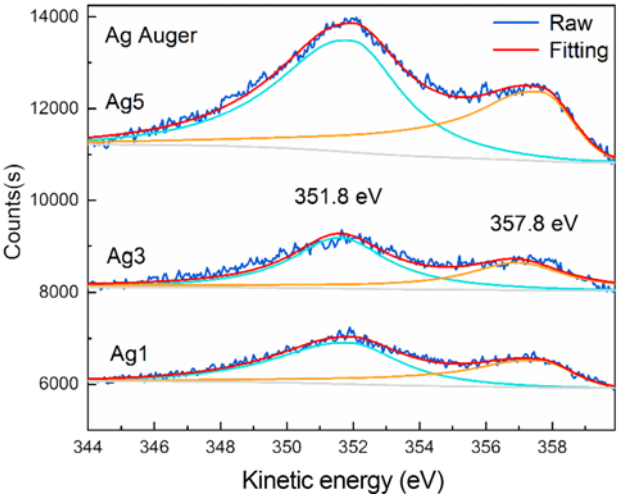

Figure 8. Auger region of Ag element of sample Ag1, Ag3 and Ag5.

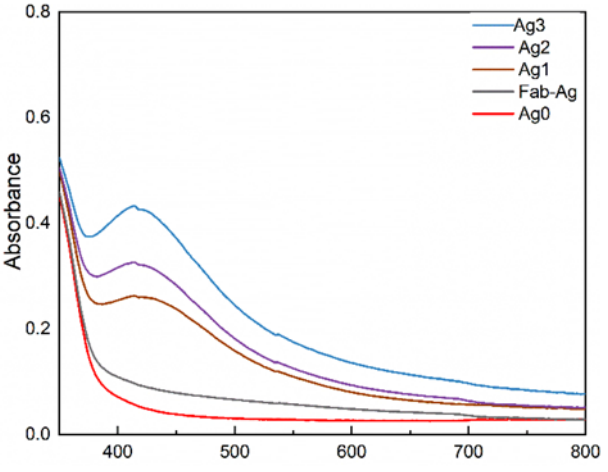

Figure 9. UV-Vis diffuse reflectance spectra (DRS) of the samples Fab-Ag, Ag0, Ag1, Ag2, and Ag3.

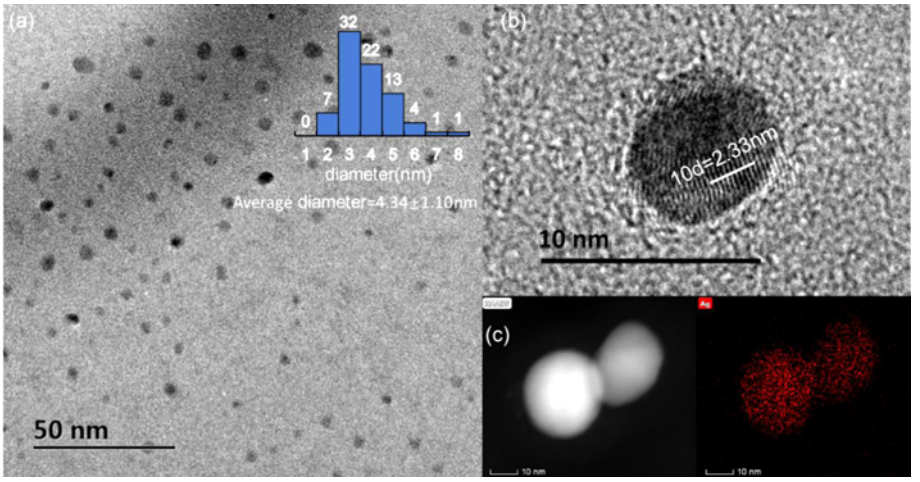

Figure 10. (a) TEM image of Ag NPs collected from the sample of Ag3 after 20 min of ultrasonic processing, (b) high-resolution TEM spectra of Ag, and (c) HAADF image and EDX mapping diagram of Ag NPs.

which indicates that the deposition of Ag NPs can be controlled by changing the concentration of the $AgNO_3$ solution.

TEM and high-resolution TEM examinations were carried out to investigate the morphology and size of the Ag NPs. For these analyses, the Ag NPs were collected from sample Ag3 after ultrasonic processing for 20 min. The TEM analysis indicated that the Ag NPs were dispersed evenly on the carbon film, and the particle count taken from Figure 10(a) confirmed the narrow distribution in average size of 2 to 9 nm. Statistics of particle size were carried out and the results are exhibited in Figure 10(a). The average diameter of Ag NPs in Ag3 is about 4.34 nm. The enlarged high-resolution TEM image in Figure 10(b) shows in more detail the Ag NPs with lattice fringes of 0.233 nm that could be indexed to the (111) plane of elemental silver (JCPDS: 04-0783), which coincides with the EDX mapping diagrams in Figure 10(c). Thus, Ag NPs were successfully in-situ synthesized on the polymer fabric by a green and effective method in this experiment, without the use of adhesives or reductive agents.

The CIELAB color space values (L*, a*, b*) of the samples Ag0, Ag1, Ag2, Ag3, Ag4 and Ag5 are shown in Table 2. The values (L*, a*, b*) of each sample was measured at five different positions, and the final results are the average of five measurements. The larger the value of b*, the more yellow the sample is. The values of b* of the samples increase significantly after loading Ag NPs, which suggests that the fiber turn to be yellow. This is due to the plasmon resonance effect on the surface of Ag NPs, which makes the fiber appear yellow after loading Ag NPs.

Figure 11 shows the results of the concentrations of the Ag ions released by the samples Ag1, Ag2, Ag3 Ag4 and Ag5 in the air-saturated DI water in the dark at room temperature at

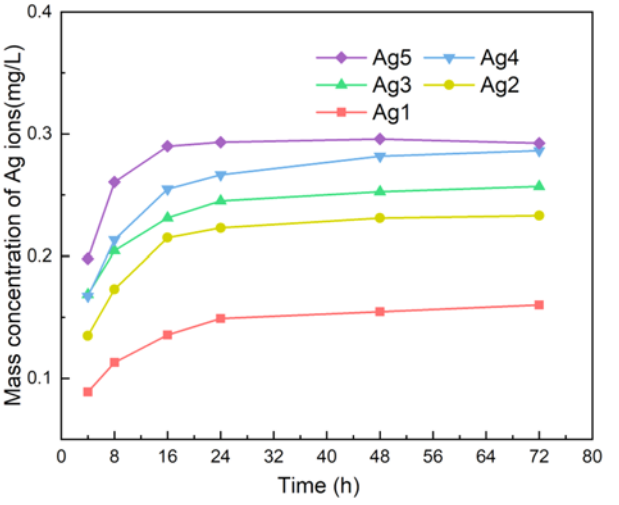

Figure 11. Concentrations of the Ag ions released by the samples Ag1, Ag2, Ag3, Ag4 and Ag5.

Table 1. Mass fraction of Ag element measured by ICP

Sample	Ag1	Ag2	Ag3	Ag4	Ag5
wt. %	0.014	0.017	0.019	0.023	0.035

different time intervals. Take 1 g samples and soak them into beakers with 100 m*l* air-saturated DI water for 4 h, 8 h, 16 h, 24 h, 48 h and 72 h. Then the content of Ag^+ in each container was tested by ICP. The measurement results show that the Ag ions are rapidly released into the aqueous solution from the fabric fiber, and the mass concentration of Ag ions in the solution achieves stability after 24 hours, indicating that the release of Ag ions in the solution has reached equilibrium. At first, Ag NPs are partially oxidized

into Ag_2O by reacting with the dissolve oxygen, and then Ag ions are released into the solution. The stability might be aroused by the consumption of dissolved oxygen in DI water.

As shown in Figure 12, the thermogravimetric curve of sample Ag3 almost overlaps with the pristine fabric. The initial degradation temperature is 420 °C, and the maximum weight loss rate is 84.5 %. The results indicate that loading Ag NPs on the fabric by the present method exhibits no significant effect on the thermodynamic properties of the fabric.

The mechanical properties of samples in different processing states are shown in the Figure 13, the tensile properties of pristine fabric, sample Ag0, sample Ag3 before H_2 DBD treatment and sample Ag3 were tested respectively. Compared with the pristine fabric, the tensile strength and elongation of the fabric after ambient air cold plasma treatment (sample Ag0) is slightly reduced. This is because plasma will etch the fiber surface and cause chain cleavage on the fiber surface during surface modification, which will affect the strength of the fiber [51,52]. As for sample Ag3 before H_2 DBD treatment and sample Ag3, the Ag_2O particles and Ag NPs nucleate and grow at the active sites on the surface of the fabric fiber, and have a certain force with the polymer molecular chain, which can strengthen the fabric to a certain extent. Therefore, after the fabric loaded with Ag_2O particles (sample Ag3 before H_2 DBD treatment) and Ag NPs (sample Ag3), the tensile strength and elongation of the fabric increased.

The antimicrobial activities of the as-prepared samples were determined by shaking-flask method. As shown in Figure 14, the sample Ag0 exhibits no antibacterial effect against either *S. aureus* or *E. coli*. Conversely, the samples Ag1, Ag2, Ag3, Ag4 and Ag5 all show antibacterial activity against both bacteria. As the content of Ag NPs increased, the sample shows better antibacterial activity, and the reduction rates of bacteria are gradually up to 99 %. The sample Ag5 exhibits best antibacterial effect against both *S. aureus* and *E. coli* due to its high Ag NPs content.

Minimum inhibitory concentration (MIC) measurements of as-prepared Ag NPs ware carried out to quantitatively

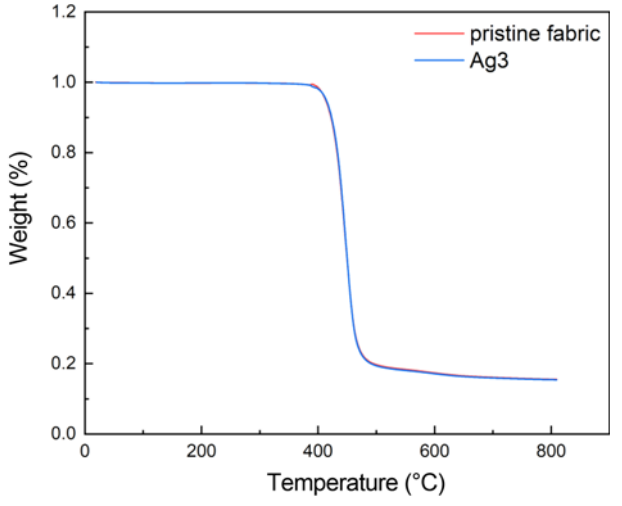

Figure 12. TG curves of the pristine fabric and sample Ag3.

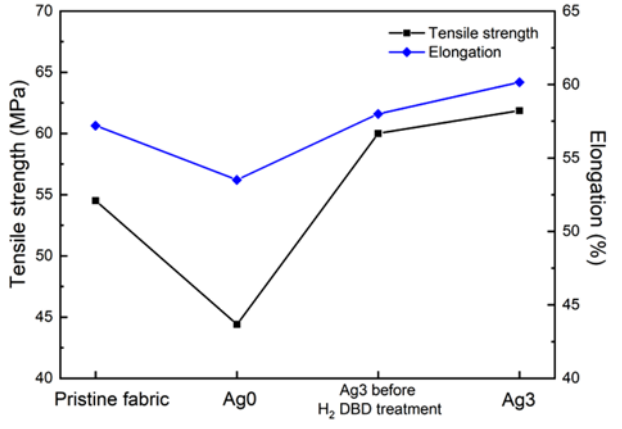

Figure 13. Tensile strength and elongation of samples in different processing states.

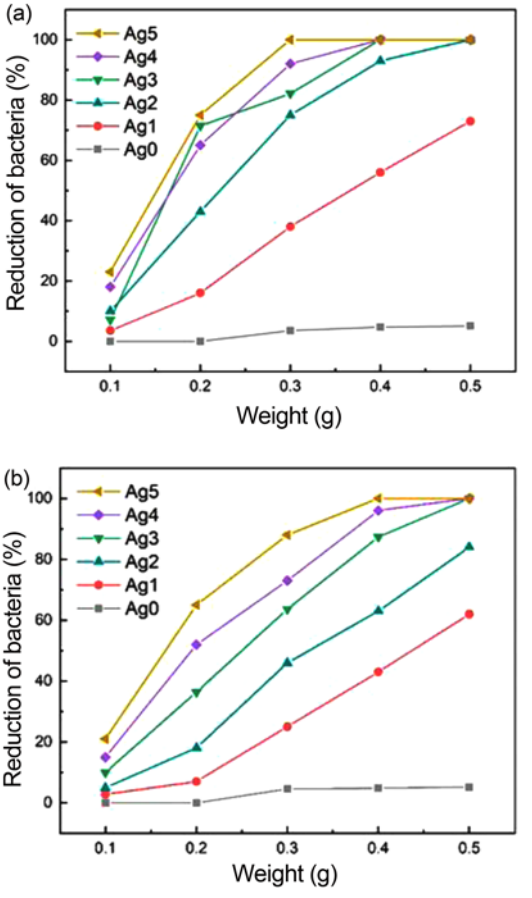

Figure 14. Variation in bacterial density in the shaking flask method; (a) *E. coli* and (b) *S. aureus*.

Table 2. CIELAB color space values (L*, a*, b*) of the samples Ag0, Ag1, Ag2, Ag3, Ag4 and Ag5

Sample	Ag0	Ag1	Ag2	Ag3	Ag4	Ag5
L*	88.93	81.85	80.20	77.17	74.53	73.26
a*	0.18	1.91	2.90	3.32	2.94	2.99
b*	3.63	12.66	11.26	13.94	13.54	15.16

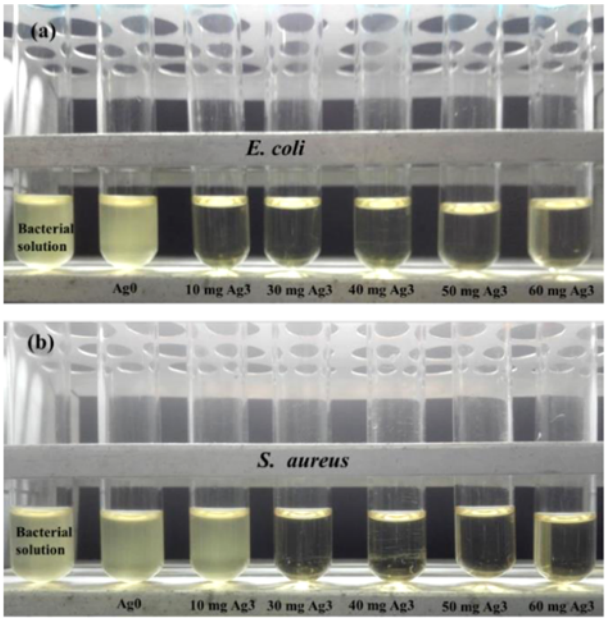

Figure 15. MIC of the sample Ag3 against (a) *E. coli* and (b) *S. aureus* in 37 °C for 20 h.

Table 3. MIC of the sample Ag3 against *Escherichia coli* and *Staphylococcus aureus* in 37 °C for 20 h

Bacterial	MIC (mg/m*l*)	
	Sample Ag3	Ag NPs
Escherichia coli	5	9.5×10^{-4}
Staphylococcus aureus	15	2.9×10^{-3}

determine the antibacterial activity of the as prepared Ag NPs. The sample Ag3 was used for assessment. The MIC values of the Ag NPs for *E. coli* and *S. aureus* in terms of the Ag NP contents were estimated by ICP, and the results are shown in Figure 15 and Table 3. It can be observed that both bacterial strains are inhibited entirely by the sample Ag3, which indicates the great antibacterial effect of the as-prepared Ag NPs composites.

The cytotoxicity of Ag NPs has been discussed in many reports [53,54]. Ag NPs at low concentration also exhibit significant antibacterial activity and exhibit no harm to human body. In vitro cytotoxicity-test revealed that Ag NPs with a concentration over 10 mg/*l* would affect the viability of epithelial cells HeLa S3 (human) [55]. Compared with the results of ICP in Table 1 and Figure 11, the Ag NPs deposited fabrics are harmless to human body.

The bacterial toxicity of Ag NPs can be derived from the particle morphology mechanism. Ag NPs with small particle size and high-energy lattice plane show a higher release rate of Ag^+, and are more toxic against bacteria [15,50]. Reactive oxygen species (ROS) generated on the surface of Ag NPs which are releasing Ag^+, could inhibit the nitrification process, and thus damage the bacterial cells [56-58].

Considerable hope has, for many years, been placed on the potential of Ag NPs as an antibacterial agent. However, the high cost and difficulties encountered in preparing Ag NPs products have kept them at the laboratory stage. In the present study, we have attempted to overcome these problems by developing a green method to prepare Ag NPs deposited fabrics, for which it is hopeful to achieve scale production. The as-prepared antibacterial fabrics possess promising applications in the medicine field as well as in human daily life for relieving the many problems caused by bacterial infections.

Conclusion

A green and innovative method was present for *in-situ* synthesis of Ag NP on hydrophobic PET fabric. The results of SEM and EDS mapping indicate that Ag element is uniformly distributed over the whole surface of PET fibers. High-resolution XPS of Ag3d and Auger, as well as the high-resolution TEM analyses confirmed that Ag only exist as the elementary substance. The as-prepared Ag NPs were deposited on the surface of the polymer fibers successfully with an average diameter of 4.34 nm. Results of TG show that the deposition of Ag NPs by this method do not change the thermostability of the substrates. The tensile strength of the Ag NPs loaded fabrics increases slightly, probably due to the hindering of crack extension by Ag NPs. Moreover, the antibacterial experiments show that the functionalized fabrics exhibited great antibacterial against both *S. aureus* and *E. coli.*. This method as a facile, short time and low energy consuming process prepares uniform distributed Ag NPs on PET fabrics with high antibacterial activity.

Acknowledgements

This work was supported by the opening foundation of the State Key Laboratory for Diagnosis and Treatment of Infectious Diseases and Collaborative Innovation Center for Diagnosis and Treatment of Infectious Diseases, The First Affiliated Hospital of Medical College, Zhejiang University, Grant No. 2017KF08, and the National Natural Science Foundation of China No. 50772098.

Electronic Supplementary Material (ESM) The online version of this article (doi: 10.1007/s12221-021-1210-8)

contains supplementary material, which is available to authorized users.

References

1. M. C. Fitzpatrick, C. T. Bauch, J. P. Townsend, and A. P. Galvani, *Nat. Microbiol.,* **4**, 1612 (2019).
2. E. Meade and M. Garvey, *Am. J. Infect. Control*, **46**, 44 (2018).
3. A. S. Gladkikh, S. I. Feranchuk, A. S. Ponomareva, N. O. Bochalgin, and L. V. Mironova, *Infect. Genetics Evol*., **78**, 104096 (2020).
4. A. Ranjan, S. Shaik, N. Nandanwar, A. Hussain, S. K. Tiwari, T. Semmler, S. Jadhav, L. H. Wieler, M. Alam, and R. R. Colwell, *mBio*, **8**, e01070-17 (2017).
5. T. Yu, G. Jiang, R. Gao, G. Chen, Y. Ren, J. Liu, H. C. van der Mei, and H. J. Busscher, *Expert Opin. Drug Deliv.,* **17**, 1151 (2020).
6. K. S. Siddiqi, A. Husen, and R. A. K. Rao, *J. Nanobiotechnol.,* **16**, 14 (2018).
7. S. Pal, Y. K. Tak, and J. M. Song, *Appl. Environ. Microbiol.*, **73** 1712 (2007).
8. V. Pareek, R. Gupta, and J. Panwar, *Mater. Sci. Eng. C*, **90**, 739 (2018).
9. N. Durán, M. Durán, M. B. de Jesus, A. B. Seabra, W. J. Fávaro, and G. Nakazato, *Biol. Med.,* **12**, 789 (2016).
10. M. Akter, M. T. Sikder, M. M. Rahman, A. K. M. A. Ullah, K. F. B. Hossain, S. Banik, T. Hosokawa, T. Saito, and M. Kurasaki, *J. Adv. Res.,* **9**, 1 (2018).
11. C. N. Lok, C. M. Ho, R. Chen, Q. Y. He, W. Y. Yu, H. Sun, P. K. Tam, J. F. Chiu, and C. M. Che, *J. Biol. Inorg. Chem.*, **12**, 527 (2007).
12. Q. B. Xu, X. T. Ke, Y. Y. Zhang, F. Y. Fu, and X. D. Liu, *Fiber. Polym.*, **19**, 2307 (2018).
13. J. Zhou, X. Hu, Y. Zhu, H. Lyu, L. Zhang, F. Fu, and X. Liu, *Cellulose,* **26**, 9323 (2019).
14. Q. B. Xu, X. T. Ke, L. W. Shen, N. Q. Ge, Y. Y. Zhang, F. Y. Fu, and X. D. Liu, *Int. J. Biol. Macromol.*, **111**, 796 (2018).
15. K. Zheng, M. I. Setyawati, D. T. Leong, and J. Xie, *Coord. Chem. Rev.,* **357**, 1 (2018).
16. S. P. Deshmukh, S. M. Patil, S. B. Mullani, and S. D. Delekar, *Mater. Sci. Eng. C*, **97**, 954 (2019).
17. Z. Y. Leng, D. R. Wu, Q. K. Yang, S. C. Zeng, and W. S. Xia, *Optik*, **154**, 33 (2018).
18. Q. Y. Chen, S. L. Xiao, S. Q. Shi, and L. P. Cai, *Polymers*, **12**, 15 (2020).
19. F. Piccapietra, L. Sigg, and R. Behra, *Environ. Sci. Technol.,* **46**, 818 (2012).
20. Q. Xu, W. Zheng, P. Duan, J. Chen, Y. Zhang, F. Fu, H. Diao, and X. Liu, *Carbohydr. Polym.*, **204**, 42 (2019).
21. P. Duan, Q. Xu, S. Shen, Y. Zhang, L. Zhang, F. Fu, and X. Liu, *Fiber. Polym.*, **20**, 1803 (2019).
22. Q. L. Chen, P. Fei, and Y. H. Hu, *Cellulose*, **26**, 8037 (2019).
23. H. Gong, M. R. Liu, and H. L. Li, *J. Mater. Sci.,* **54**, 6895 (2019).
24. Y. P. Wu, Y. Yang, Z. J. Zhang, Z. H. Wang, Y. B. Zhao, and L. Sun, *Text. Res. J.,* **89**, 867 (2019).
25. H. M. Fahmy, A. A. Aly, and A. Abou-Okeil, *Int. J. Biol. Macromol.,* **114**, 929 (2018).
26. R. Liu, L. Dai, C. Si, and Z. Zeng, *Carbohydr. Polym.,* **195**, 63 (2018).
27. M. Liu, X. P. Duan, Y. M. Li, D. P. Yang, and Y. Z. Long, *Mater. Sci. Eng. C*, **76**, 1413 (2017).
28. C. Cheng, Z. Liye, and R. J. Zhan, *Surf. Coat. Tech.,* **200**, 6659 (2006).
29. C. Liu, J. Liu, X. Ning, S. Chen, Z. Liu, S. Jiang, and D. Miao, *Polymers*, **11**, 627 (2019).
30. P. Kord Forooshani, E. Polega, K. Thomson, M. S. A. Bhuiyan, R. Pinnaratip, M. Trought, C. Kendrick, Y. Gao, K. A. Perrine, L. Pan, and B. P. Lee, *Front. Chem.,* **7**, 631 (2019).
31. A. M. Wróbel, M. Kryszewski, W. Rakowski, M. Okoniewski, and Z. Kubacki, *Polymer*, **19**, 908 (1978).
32. R. Morent, N. De Geyter, J. Verschuren, K. De Clerck, P. Kiekens, and C. Leys, *Surf. Coat. Tech.,* **202**, 3427 (2008).
33. M. Simor, J. Rahel, P. Vojtek, M. Cernak, and A. Brablec, *Appl. Phys. Lett*., **81**, 2716 (2002).
34. H. Al-Maliki, L. Zsidai, P. Samyn, Z. Szakál, R. Keresztes, and G. Kalácska, *Polym. Eng. Sci.,* **58**, 93 (2018).
35. W. Ren, C. Cheng, R. Wang, and X. Li, *J. Appl. Polym. Sci.,* **116**, 2480 (2010).
36. M. E. El-Naggar, T. A. Khattab, M. S. Abdelrahman, A. Aldalbahi, and M. R. Hatshan, *Cellulose*, https://doi.org/10.1007/s10570-020-03537-4 (2020).
37. X. L. Deng, A. Nikiforov, D. Vujosevic, V. Vuksanovic, B. Mugoša, U. Cvelbar, N. DeGeyter, R. Morent, and C. Leys, *Mater. Lett.,* **149**, 95 (2015).
38. Y. Zhou, Z. Sun, L. Jiang, S. Chen, J. Ma, and F. Zhou, *Appl. Surf. Sci.,* **533**, 147431 (2020).
39. C. Mandolfino, *Surf. Coat. Technol.,* **336**, 331 (2019).
40. M. Vajpayee, M. Singh, L. Ledwani, R. Prakash, and S. K. Nema, *ACS Omega*, **5**, 19034 (2020).
41. R. Morent, N. De Geyter, C. Leys, L. Gengembre, and E. Payen, *Surf. Coat. Technol.*, **201**, 7847 (2007).
42. A. A. Azanova, I. A. Borodaev, V. S. Zheltukhin, and A. A. Shakhyrov, *Bull. Russian Acad. Sci. Phys.*, **82**, 189 (2018).
43. G. Poletti, F. Orsini, A. Raffaele-Addamo, C. Riccardi, and E. Selli, *Appl. Surf. Sci.,* **219**, 311 (2003).
44. A. Bogaerts, E. Neyts, R. Gijbels, and J. van der Mullen, *Spectroc. Acta Pt. B-Atom. Spectr.,* **57**, 609 (2002).
45. X. D. Cheng, P. M. Dong, Z. F. Huang, Y. Z. Zhang, Y. Chen, and X. X. Nie, *J. CO_2 Util.,* **20**, 200 (2017).
46. J. M. Mariot and G. J. Dufour, *Electron. Spectrosc. Relat. Phenom.*, **13**, 403 (1978).
47. G. Schoen, *Acta Chem. Scand.*, **27**, 2623 (1973).
48. P. C. Nagajyothi, S. V. Prabhakar Vattikuti, K. C. Devarayapalli,

K. Yoo, J. Shim, and T. V. M. Sreekanth, *Crit. Rev. Environ. Sci. Technol.,* **50**, 2617 (2020).
49. T. Abou Elmaaty, K. El-Nagare, S. Raouf, K. Abdelfattah, S. El-Kadi, and E. Abdelaziz, *RSC Adv.,* **8**, 25546 (2018).
50. A. M. Eremenko, I. S. Petrik, N. P. Smirnova, A. V. Rudenko, and Y. S. Marikvas, *Nanoscale Res. Lett.,* **11**, 28 (2016).
51. X. Song, U. Cvelbar, P. Strazar, L. Vossebein, and A. Zille, *Polymers*, **11**, 1769 (2019).
52. J. Yip, K. Chan, K. M. Sin, and K. S. Lau, *J. Mater. Proc. Technol.*, **123**, 5 (2002).
53. S. Chernousova and M. Epple, *Angew. Chem. Int. Ed.*, **44**, 1636 (2013).
54. R. Muhammad, K. Zakia, R. Anum, S. Anjum, R. Saira, and N. Shahzad, *Nanomaterials*, **6**, 74 (2016).
55. T. H. Kim, M. Kim, H. S. Park, U. S. Shin, M. S. Gong, and H. W. Kim, *J. Biomed. Mater. Res. Part A,* **100**, 1033 (2012).
56. W. Zhang, B. Xiao, and T. Fang, *Chemosphere*, **191**, 324 (2018).
57. J. Liu and R. H. Hurt, *Environ. Sci. Technol.,* **44**, 2169 (2010).
58. M. A. Raza, Z. Kanwal, A. Rauf, A. N. Sabri, S. Riaz, and S. Naseem, *Nanomaterials (Basel)*, **6**, 74 (2016).